



HAL
open science

Tsunami hazard assessment in the Makran subduction zone

Amin Rashidi, Zaher Hossein Shomali, Denys Dutykh, Nasser Keshavarz Faraj
Khah

► **To cite this version:**

Amin Rashidi, Zaher Hossein Shomali, Denys Dutykh, Nasser Keshavarz Faraj Khah. Tsunami hazard assessment in the Makran subduction zone. *Natural Hazards*, 2020, 100, pp.861-875. 10.1007/s11069-019-03848-1 . hal-01737767v2

HAL Id: hal-01737767

<https://hal.science/hal-01737767v2>

Submitted on 29 Mar 2018

HAL is a multi-disciplinary open access archive for the deposit and dissemination of scientific research documents, whether they are published or not. The documents may come from teaching and research institutions in France or abroad, or from public or private research centers.

L'archive ouverte pluridisciplinaire **HAL**, est destinée au dépôt et à la diffusion de documents scientifiques de niveau recherche, publiés ou non, émanant des établissements d'enseignement et de recherche français ou étrangers, des laboratoires publics ou privés.



Distributed under a Creative Commons Attribution - NonCommercial - ShareAlike 4.0 International License

Tsunami hazard assessment in the Makran subduction zone

Amin RASHIDI^{1*}, Zaher Hossein SHOMALI^{1,2}, Denys DUTYKH^{3,4} and Nasser KESHAVARZ FARAJKHAH⁵

¹ Institute of Geophysics, University of Tehran, Tehran, Iran

² Department of Earth Sciences, Uppsala University, Uppsala, Sweden

³ Univ. Grenoble Alpes, Univ. Savoie Mont Blanc, CNRS, LAMA, 73000 Chambéry, France

⁴ LAMA UMR 5127 CNRS, Université Savoie Mont Blanc, Campus Scientifique, 73376 Le Bourget-du-Lac, France

⁵ Research Institute of Petroleum Industry, Tehran, Iran

Abstract. The lack of offshore seismic data caused uncertainties associated to understating the behavior of future tsunamigenic earthquakes in the MAKRAN Subduction Zone (MSZ). Future tsunamigenic events in the MSZ may trigger significant near-field tsunamis. Run-up heights in the near-field are controlled by the heterogeneity of slip over the rupture area. Considering a non-planar geometry for the MAKRAN subduction zone, a range of random k^{-2} slip models were generated to hypothesize rupturing on the fault zone. We model tsunamis numerically and assess probabilistic tsunami hazard in the near-field for all synthetic scenarios. The main affected areas by tsunami waves are the area between JASK and ORMARA along the shorelines of IRAN and PAKISTAN and the area between MUSCAT and SUR along the OMAN coastline. The maximum peak-run-up along the shores of IRAN and PAKISTAN is about 16 m and about 12 m for the OMAN shoreline. The slip distributions control the run-up along the MAKRAN coastlines. The dependency of run-up to the heterogeneity of slip is higher in the most impacted areas. Those areas are more vulnerable to tsunami hazard than other areas.

Keywords: MAKRAN subduction zone; wave run-up; heterogeneity of slip; numerical tsunami modeling; probabilistic tsunami hazard assessment.

1 Introduction

The MAKRAN Subduction Zone (MSZ) is a convergent plate boundary between the ARABIAN plate and the overlying EURASIAN plate with an average convergent rate of ~ 4 cm/yr. It extends about 900 km from southeastern IRAN to southern PAKISTAN. The 1945 MAKRAN tsunami and the possibility of generating future tsunamigenic events by the MAKRAN subduction zone have motivated researches recently to study tsunami hazard in the northwestern INDIAN OCEAN (*e.g.* Okal and Synolakis, 2008; Heidarzadeh *et al.*, 2008a; Rajendran *et al.*, 2008; Heidarzadeh and Kijko, 2011; Rehman *et al.*, 2013; El-Hussain *et al.*, 2016; Hoechner *et al.*, 2016).

The occurrence of the 1945 MAKRAN and the evidences of earlier historic earthquakes (*e.g.* 1008 and 1483) have proved earthquake and tsunami potential of the MAKRAN subduction zone (Byrne *et al.*, 1992; Heidarzadeh *et al.*, 2008a; Smith *et al.*, 2013). It is seismically active, being capable of generating large earthquakes. However, it is segmented into the western and eastern parts from the seismic potential point of view. The active eastern segment generated the 1945 tsunamigenic earthquake (M_w 8.1) which caused a regional tsunami with maximum wave heights of 10 m and about 4 000 human losses (Heidarzadeh *et al.*, 2008b; Rajendran *et al.*,

* Corresponding author. E-mail address: amin.rashidi@ut.ac.ir (A. RASHIDI).

2013). The potential of the western segment for generating tsunamigenic earthquakes is puzzling due to its apparent aseismicity and the lack of historical data. There has been some confusion in the studies on which behavior can explain the current status of the western MAKRAN. The presence of sediment layers may be the cause of unusual seismic behavior of the western MAKRAN. Until the end of 2004, previous investigations have suggested that the SUMATRA subduction zone, at least the northern part, was considered to be sleeping from which tsunamigenic events would not be expected. The lack of historic data on major seismic events during the last 200 years was supporting this misconception. The gigantic 2004 SUMATRA ANDAMAN earthquake strongly disproved this belief. After more thorough investigations, the traces of major tsunamis have been found in sediment deposits on the horizon of 1000 years. The same story may happen to the MSZ, especially for the western segment. The duration of our seismic records and observations is not enough to predict reliably earthquakes on long term. Another example is the recent TŌHOKU 2011 tsunamigenic event. The FUKUSHIMA nuclear plant was protected against tsunamis, but the chosen tsunami design height was twice smaller than the real wave which hit the plant. One can assume that the western segment is currently locked and capable of generating future plate boundary earthquakes (Musson, 2009; Rajendran *et al.*, 2013). This assumption leads to serious reconsideration of the entire MAKRAN rupturing scenario. MAKRAN subduction zone is characterized as a shallow subduction zone which can increase coupling and provide a suitable condition to release large earthquakes (Gutscher and Westbrook, 2009; Smith *et al.*, 2012).

The 2004 INDIAN OCEAN and 2011 TŌHOKU tsunamis have demonstrated that the scale and impacts of tsunamis can be significantly larger than expected (Suppasri *et al.*, 2013; Satake, 2014) showing the need of increasing attention to the hazard potential of subduction zones for worst case scenarios.

The effect of far-field tsunamis can be suitably evaluated knowing the seismic moment M_0 of the submarine earthquake (Dutykh *et al.*, 2012). However, the tsunami hazard of tsunamigenic earthquakes in the near field depends on several factors which have increased the researchers interest recently (*e.g.* Dutykh *et al.*, 2011; Lay *et al.*, 2011; Yamazaki and Cheung, 2011; Yamazaki *et al.*, 2011; Dutykh *et al.*, 2012). Although, the tsunami propagation *per se* is well modeled and understood, it can be still problematic due to uncertainties in the rupture details (Greenslade and Titov, 2008). As a lesson from the 2004 INDIAN OCEAN and 2011 TŌHOKU tsunamis, the tsunami generation process and its relationship with seismogenic subduction zones need to be investigated in more detail (Fujii *et al.*, 2011; Ide *et al.*, 2011). The tsunami generation simulation is the controlling step in modeling the life stages of tsunamis and their effects on coastal areas. In the case of tectonic-generated tsunamis, rupture geometry, focal mechanism, seismic moment and coseismic slip distribution describe the tsunami generation process. They are required to compute the 3D seafloor deformation caused by rupturing on an underwater fault. Tsunami numerical modeling may fail to predict the true effects of tsunamis by assuming simple uniform slip distributions. Heterogeneity of slip over the fault controls local tsunami wave amplitude variations (Geist and Dmowska, 1999), which is necessary to model near-field tsunamis accurately and assess their hazard.

Tsunami hazard can be assessed in three different approaches (González *et al.*, 2009): (1) Probabilistic Tsunami Hazard Assessment (PTHA), (2) worst-case scenario approach (deterministic), and (3) sensitivity analysis. The last one (see *e.g.* Tang *et al.*, 2006; Barkan *et al.*, 2009) studies the sensitivity of flooding or run-up to the characteristics of tsunami sources which does not consider the probability of each scenario (González *et al.*, 2009; Dutykh *et al.*, 2011).

Deterministic approach (*e.g.* Parsons, 2008; Priest *et al.*, 2009) considers particular scenarios (usually the worst case scenario) to calculate their effect on specific areas. Probabilistic Tsunami Hazard Assessment (PTHA) provides a useful tool to evaluate tsunami risk by considering the probabilities of tsunamis. It determines the likelihood of tsunami severity usually in terms of tsunami run-up or flooding for a range of possible sources. PTHA computes the probability of tsunami run-up or inundation at a given location that exceeds a certain level in a specified time period. It was developed by Lin and Tung (1982), Rikitake and Aida (1988) and Downes and Stirling (2001) by modifying the probabilistic seismic hazard assessment (PSHA). Increased attention has been paid recently to PTHA, especially after the 2004 INDIAN OCEAN tsunami (*e.g.* Geist and Parsons, 2006; González *et al.*, 2009; Grezio *et al.*, 2012; Sørensen *et al.*, 2012; Horspool *et al.*, 2014). PTHA in MAKRAN has been also a subject of interest to some researchers (*e.g.* Heidarzadeh and Kijko, 2011; El-Hussain *et al.*, 2016; Hoechner *et al.*, 2016).

In our previous study (Rashidi *et al.*, 2018), the evolution of kinetic, potential and total energies in the near-field was studied for a multi-segment source model of the MAKRAN subduction zone. An empirical relationship between the moment magnitude and tsunami wave energy in the MAKRAN subduction zone was obtained. In the current study, we model hypothetical earthquakes generated by the entire MAKRAN subduction zone and perform PTHA. Heterogeneous slip distribution patterns are considered to represent the complexity of earthquakes. Spatial non-uniform slip models are a better approximation of the rupture complexity to model seismic sources (Ruiz *et al.*, 2015), however, it is ignored in many tsunami studies assuming simple source models (Geist, 2002). The current study is focused on the k^{-2} rupture model, introduced by Bernard and Herrero (1994) and developed by Gallovič and Brokešová (2004). The distributions of run-up along the shores of IRAN, PAKISTAN and OMAN are used in our analysis and assessment.

2 Methodology

2.1 Earthquake source models

Heterogeneity of slip in plate boundary events greatly impacts the vertical seabed displacement and thus the tsunami generation (Geist, 2002). The lack of offshore seismic data has limited our understanding of the present-day behavior of the MAKRAN subduction zone and insight into the complexity of slip distribution of possible future events. Alternatively, synthetic slip models can be useful tools to exhibit the complexity of tsunamigenic sources and to understand their effects in the MAKRAN region. Using k^{-2} stochastic source models, we generate digital static tsunamigenic ruptures to model near-field tsunamis. Bernard and Herrero (1994) proposed the so-called *kinematic self-similar rupture model* in which spectral

amplitudes of a random slip distribution decay as power of 2 at high wave numbers k beyond the corner wavenumber $k_c = 1/L_c$, where L_c is the characteristic dimension of the fault (usually the length) (Galovič and Brokešová, 2004). The slip does not depend on k below k_c . In the case of a rectangular fault with a length of L and a width of W , the 2D slip distribution $D(k_x, k_z)$ can be written as its spatial FOURIER spectrum (Galovič and Brokešová, 2004)

$$D(k_x, k_z) = \frac{\Delta\bar{u} L W}{\sqrt{1 + \left(\left(\frac{k_x L}{K} \right)^2 + \left(\frac{k_z W}{K} \right)^2 \right)}} e^{i\Phi(k_x, k_z)}, \quad (1)$$

where $\Delta\bar{u}$ is the mean slip and $\Phi(k_x, k_z)$ is the phase spectrum, k_x and k_z are the wavenumber components along the x and z directions and K is a dimensionless constant which determines the smoothness of slip distribution (Galovič and Brokešová, 2004). Based on Somerville *et al.* (1999), $K < 1$ is suggested, which corresponds to smoother slip distributions.

To define rupture scenarios, a non-planar fault geometry (Figure 1) is constructed by modifying the plate interface and deformation front from Smith *et al.* (2013). The southwest apex of the fault is located at 24.62°N and 57.68°E. The width of the fault is 210 km, which correspond to the limit of significant offshore seismicity (Smith *et al.*, 2013). Smith *et al.* (2013) presented three potential rupture scenarios in the MAKRAN region including the full length of the MAKRAN subduction zone, eastern MAKRAN segment and SISTAN suture zone to LITTLE MURRAY Ridge. They considered a coseismic slip of 10 m for each scenario. Motivated by this work and considering a range of uncertainty, 100 random heterogeneous k^{-2} slip distributions are generated for hypothetical earthquakes using 10 ± 1 m of mean coseismic slip and $K = 0.5 \pm 0.2$. Figure 2 shows one of k^{-2} slip distributions for the MAKRAN subduction rupture, for instance.

2.2 Tsunami numerical modeling

To provide the initial condition for tsunami modeling of earthquake scenarios, the seabed static deformation is computed using the OKADA solution (Okada, 1985) (Figure 2). We simulate tsunamis using the COMCOT numerical model (Liu *et al.*, 1998) which uses explicit staggered leapfrog finite difference schemes to solve both linear and non-linear shallow water equations in both spherical and CARTESIAN coordinates. COMCOT is a well-known and validated numerical tool that is used widely for investigating near-field and far-field tsunamis (*e.g.* Wang and Liu, 2005, 2006; Barkan and ten Brink, 2010; Heidarzadeh and Satake, 2014). All simulations are performed for a total run time of 10 h with a time discretization step of 2 s. The bottom friction is considered in the simulations. Nonlinear shallow water equations are discretized in spherical coordinates. Tsunami inundation on dry land is not computed due to the lack of high-resolution local bathymetry and topography data. Therefore, we have to use a global bathymetry grid for our purpose. The GEBCO 30 arcsec bathymetry data (Smith and Sandwell, 1997; Becker *et al.*, 2009), available at <http://www.gebco.net/>, is used for our simulations.

2.3 Tsunami hazard assessment

The run-up distributions along the shorelines of IRAN, PAKISTAN and OMAN resulted from tsunami modeling of heterogeneous slip models are used to assess the probabilistic tsunami hazard. Computing annual rate of earthquakes as tsunami generators is required in PTHA. The truncated GUTENBERG–RICHTER relation (Cosentino *et al.*, 1977; Weichert, 1980) is applied to compute the annual number of the earthquakes (Figure 3) using events from 1926 – 2016 driven from the ISC catalog (Figure 1). Applying the maximum likelihood method (Weichert, 1980), the resulting magnitude of completeness is 4.7 and the b -value 0.8. The b -value is the slope of line in the GUTENBERG–RICHTER relation and represents the relative abundance of large to small events. We consider a maximum magnitude of 9.2 based on Smith *et al.* (2013).

The occurrence of tsunamigenic earthquake scenarios is assumed to be a POISSONIAN process. The probability of tsunami wave amplitude ζ exceeding a specific value ζ_c at a given coastline in a time period T for a total number N of tsunamigenic sources can be written as

$$\mathbb{P}(\zeta \geq \zeta_c) = 1 - \prod_{i=1}^N [1 - (1 - e^{-v_i T}) \mathbb{P}(\zeta \geq \zeta_c | S_i)]. \quad (2)$$

where v_i is the annual occurrence rate of i^{th} scenario S_i and $\mathbb{P}(\zeta \geq \zeta_c | S_i)$ is the probability that tsunami wave amplitude ζ resulted from i^{th} scenario S_i exceeds the given value ζ_c which is 1 if $\zeta \geq \zeta_c$ and 0 if $\zeta < \zeta_c$.

3 Results

Figure 4 shows run-up distributions from all scenarios along the coastlines of IRAN and PAKISTAN. The computed mean, lower and upper run-up bounds along the coastlines of IRAN and PAKISTAN are also represented in Figure 4. The same results for the coastline of OMAN are shown in Figure 5. The mean run-up along the shores of IRAN and PAKISTAN ranges between 0 and 7 m, while it changes between 0 and 6 m along the OMAN coast. The maximum run-up reaches a height of ~ 16 m along the shores of IRAN and PAKISTAN and ~ 12 m for the OMAN shoreline. The run-up attenuates to the West and East of the IRAN – PAKISTAN shoreline. The highest run-up values along the shore are observed near the ports of CHABAHAR and JIWANI. In the case of OMAN coast, an area between MUSCAT and South of SUR encounters the largest wave heights. Run-up heights attenuate to the South of OMAN coastline, especially around the MASIRAH ISLAND. Table 1 shows the estimated mean and maximal run-up heights in some major coastal cities along the shores of IRAN, PAKISTAN and OMAN.

Figure 6 shows histograms of run-up heights along the coastlines of IRAN, PAKISTAN and OMAN and at several selected ports. About 90 % of tsunami waves cause a run-up height up to 4 m. Among the selected locations, CHABAHAR is impacted by a larger number of higher run-up heights. JASK is exposed to the least hazard with maximum wave heights mainly from 1 to 2 m.

The results of PTHA are presented in Figures 7 – 9. Figure 7 shows the probability of tsunami wave amplitude exceeding 3 m evaluated for coastlines of IRAN,

<i>City</i>	<i>Mean estimated run-up (m)</i>	<i>Maximal run-up (m)</i>
JASK	1	2
KONARAK	4	11
CHABAHAR	5	10
JIWANI	2	5
PASNI	3	6
ORMARA	4	8
MUSCAT	5	8
SUR	5	9

Table 1. *Estimated mean and maximal run-up heights in major coastal cities along the coastlines of IRAN, PAKISTAN and OMAN.*

PAKISTAN and OMAN in time periods of 50, 250 and 1 000 years. Distributions of the exceedance probability in 50, 250 and 1 000 years illustrate a relatively similar pattern along the shorelines. The probability of exceeding 3 m increases with time. However, its changes in the West and East of IRAN – PAKISTAN shoreline and West of MUSCAT are insignificant. For a region between JASK and ORMARA along the IRAN – PAKISTAN shoreline, the probability of exceedance is high. It ranges from 0 to 0.56 in 50 years and reaches to 1 in 1 000 years for most locations between JASK and ORMARA. The exceedance probability is significant between MUSCAT and SUR, ranging from 0 to 0.99 (~ 1) in 250 years. It decreases to less than 0.11 to the West of MUSCAT.

Figure 8 shows the probability of exceeding different wave heights at one or more locations along the coastlines of IRAN and PAKISTAN and OMAN in time periods of 50, 250 and 1 000 years. The same plots for the annual probability are displayed in Figure 9. For both coastlines of IRAN – PAKISTAN and OMAN, the value of exceedance probability for 3 m is about 0.6 in 50 years and 1 in 250 and 1 000 years. The probability that tsunami wave height exceeds 9 m at at least one location along the IRAN – PAKISTAN shoreline is 0.33, 0.86 and 1 during 50, 250 and 1 000 years, respectively. The same values for the coast of OMAN are 0.11, 0.43 and 0.9. The annual exceedance probability for tsunami wave heights between 1 and 5 m is a constant value of 0.018. It falls exponentially for higher tsunami heights.

4 Discussion and Conclusions

Taking into account a range of near-field source models, our tsunami simulations show that maximum run-up reaches to a height of 16 m along the coastlines of IRAN and PAKISTAN. The minimum bound of run-up exhibits a relative uniform distribution which can match with run-up from a uniform slip distribution (Ruiz *et al.*, 2015). The results of our simulations show that near-field run-up along the coastlines depends on the slip distribution of tsunamigenic events. Different slip models result in different patterns of run-up along the shores, especially for the zones located parallel to the rupture area. The patterns of run-up from non-uniform

slip distributions are more complex than uniform slip distributions. Moreover, the resolution of bathymetry can largely affect run-up heights. Clearly, the higher resolution bathymetry grid has, the more accurate run-up computation is. Besides the different slip distributions, the non-uniform shape of the IRAN – PAKISTAN coastline due to the presence of different coastal features influences the pattern of run-up. A high variability of run-up heights can be seen between 58.5°E and 65.3°E , which corresponds to the concentration of slip over the rupture area. This part of the shore is the most affected area by tsunamis. To the West and East of IRAN – PAKISTAN shoreline, the dependency of run-up to the heterogeneity of slip relatively decreases. It reflects a lower uncertainty of run-up in these areas.

For the coast of OMAN, the variability of run-up is high in an area between MUSCAT and SUR. The uncertainty of run-up showed by lower and upper run-up bounds is lower in other parts of the OMAN shore. To the South of OMAN's eastern tip, run-up heights are highly attenuated around the MASIRAH ISLAND because of the tsunami waves scattering. However, it seems that run-up values amplify locally to the South of the MASIRAH ISLAND due to multiple reflections of tsunami waves.

The probabilistic tsunami hazard for the central part of IRAN – PAKISTAN shoreline and the area between MUSCAT and SUR is quite considerable. Tsunami waves deplete their energy mainly along those areas. The location of western and eastern parts of IRAN – PAKISTAN shoreline and the West of MUSCAT with respect to the extent of slip on the fault area causes very weaker run-up heights and thus lower levels of tsunami hazard in comparison to the central areas. Scattering of tsunami waves around OMAN's eastern tip can dissipate tsunami waves energy and cause attenuated run-up to the South of OMAN. While the tsunami hazard probability increases with time along the most affected areas, it stays nearly constant in other areas. The short-term (50 years), mid-term (250 years) and long-term ($\sim 1\,000$ years) tsunami hazard along the main affected areas are significant which make them highly vulnerable to tsunami hazard. Other areas are less susceptible to tsunami hazard. Tsunami hazard variability with time depends on size and magnitude of tsunamigenic scenarii. This study presumes a certain size of the MAKRAN rupture area with a limited range of magnitudes. Considering different sizes of rupture areas with different magnitudes will change the results. In general, IRAN is more vulnerable than PAKISTAN and OMAN to tsunami hazard from the entire MAKRAN subduction zone. High run-up heights are distributed along a broader area for the IRANIAN part of the shoreline.

This study takes into account the effect of slip heterogeneity on tsunami hazard along the shorelines of IRAN, PAKISTAN and OMAN considering a range of uncertainty for mean slip value and slip distribution. Future works should consider the effects of other factors on run-up along those coastlines (*e.g.* fault parameters, the dynamic bottom motion, other near-field and far-field tsunamigenic sources, *etc.*). Besides, high resolution site-specific bathymetric/topographic maps are required to improve the results of our study and to compute the tsunami inundation of dry land.

The high level long-term tsunami hazard of MAKRAN subduction zone indicates the need of preparedness for future events especially by developing a regional tsunami early warning system for MAKRAN coastlines. Special attention needs to be paid to the central part of IRAN – PAKISTAN shoreline and the area between

MUSCAT and SUR. Local authorities might be interested to use the results of this study alongside with other relevant publications in order to increase the protection level of coastal facilities. The MAKRAN subduction zone is a common threat for different countries, especially IRAN, OMAN, PAKISTAN and INDIA. Collaborative studies, sharing data and tsunami awareness education can constructively mitigate the MAKRAN tsunami hazard.

References

- Barkan, R. and ten Brink, U. (2010). Tsunami simulations of the 1867 Virgin Island earthquake: Constraints on epicenter location and fault parameters. *Bulletin of the Seismological Society of America*, 100(3):995–1009. 4
- Barkan, R., ten Brink, U. S., and Lin, J. (2009). Far field tsunami simulations of the 1755 Lisbon earthquake: Implications for tsunami hazard to the U.S. East Coast and the Caribbean. *Marine Geology*, 264(1-2):109–122. 3
- Becker, J. J., Sandwell, D. T., Smith, W. H. F., Braud, J., Binder, B., Depner, J., Fabre, D., Factor, J., Ingalls, S., Kim, S.-H., Ladner, R., Marks, K., Nelson, S., Pharaoh, A., Trimmer, R., Rosenberg, J. V., Wallace, G., and Weatherall, P. (2009). Global bathymetry and elevation data at 30 arc seconds resolution: Srtm30_plus. *Marine Geodesy*, 32(4):355–371. 4
- Bernard, P. and Herrero, A. (1994). Slip heterogeneity, body-wave spectra, and directivity of earthquake ruptures. *Annali di Geofisica*, XXXVII:1679–1690. 3
- Byrne, D. E., Sykes, L. R., and Davis, D. M. (1992). Great thrust earthquakes and aseismic slip along the plate boundary of the Makran Subduction Zone. *Journal of Geophysical Research*, 97(B1):449. 1, 12
- Cosentino, P., Ficarra, V., and Luzio, D. (1977). Truncated exponential frequency-magnitude relationship in earthquakes statistics. *Bulletin of the Seismological Society of America*, 67(6):1615–1623. 5
- Downes, G. L. and Stirling, M. W. (2001). Groundwork for development of a probabilistic tsunami hazard model for New Zealand. In Bernard, E., editor, *International Tsunami Symposium 2001*, pages 293–301. Pacific Marine Environmental Lab., Seattle, Wash. 3
- Dutykh, D., Labart, C., and Mitsotakis, D. (2011). Long wave run-up on random beaches. *Physical Review Letters*, 107(18):184504. 2, 3
- Dutykh, D., Mitsotakis, D., Chubarov, L. B., and Shokin, Y. I. (2012). On the contribution of the horizontal sea-bed displacements into the tsunami generation process. *Ocean Modelling*, 56:43–56. 2
- El-Hussain, I., Omira, R., Deif, A., Al-Habsi, Z., Al-Rawas, G., Mohamad, A., Al-Jabri, K., and Baptista, M. A. (2016). Probabilistic tsunami hazard assessment along Oman coast from submarine earthquakes in the Makran subduction zone. *Arabian Journal of Geosciences*, 9(15):668. 1, 3
- Fujii, Y., Satake, K., Sakai, S., Shinohara, M., and Kanazawa, T. (2011). Tsunami source of the 2011 off the Pacific coast of Tohoku Earthquake. *Earth, Planets and Space*, 63(7):815–820. 2
- Gallovič, F. and Brokešová, J. (2004). The k-2 rupture model parametric study: Example of the 1999 Athens earthquake. *Studia Geophysica et Geodaetica*, 48(3):589–613. 3, 4

- Geist, E. L. (2002). Complex earthquake rupture and local tsunamis. *Journal of Geophysical Research*, 107(B5):2086. 3
- Geist, E. L. and Dmowska, R. (1999). Local Tsunamis and Distributed Slip at the Source. *Pure and Applied Geophysics*, 154(3-4):485–512. 2
- Geist, E. L. and Parsons, T. (2006). Probabilistic analysis of tsunami hazards. *Natural Hazards*, 37(3):277–314. 3
- González, F. I., Geist, E. L., Jaffe, B., Kânolu, U., Mofjeld, H., Synolakis, C. E., Titov, V. V., Areas, D., Bellomo, D., Carlton, D., Horning, T., Johnson, J., Newman, J., Parsons, T., Peters, R., Peterson, C., Priest, G., Venturato, A., Weber, J., Wong, F., and Yalciner, A. (2009). Probabilistic tsunami hazard assessment at Seaside, Oregon, for near-and far-field seismic sources. *Journal of Geophysical Research: Oceans*, 114(11):C11023. 3
- Greenslade, D. J. and Titov, V. V. (2008). A comparison study of two numerical tsunami forecasting systems. *Pure and Applied Geophysics*, 165(11-12):1991–2001. 2
- Grezio, A., Gasparini, P., Marzocchi, W., Patera, A., and Tinti, S. (2012). Tsunami risk assessments in Messina, Sicily - Italy. *Natural Hazards and Earth System Science*, 12(1):151–163. 3
- Gutscher, M.-A. and Westbrook, G. K. (2009). Great Earthquakes in Slow-Subduction, Low-Taper Margins. In Lallemand, S. and Funiciello, F., editors, *Subduction Zone Geodynamics*, pages 119–133, Berlin, Heidelberg. Springer Berlin Heidelberg. 2
- Heidarzadeh, M. and Kijko, A. (2011). A probabilistic tsunami hazard assessment for the Makran subduction zone at the northwestern Indian Ocean. *Natural Hazards*, 56(3):577–593. 1, 3
- Heidarzadeh, M., Pirooz, M. D., Zaker, N. H., and Synolakis, C. E. (2008a). Evaluating tsunami hazard in the Northwestern Indian Ocean. *Pure and Applied Geophysics*, 165(11-12):2045–2058. 1
- Heidarzadeh, M., Pirooz, M. D., Zaker, N. H., Yalciner, A. C., Mokhtari, M., and Esmaeily, A. (2008b). Historical tsunami in the Makran Subduction Zone off the southern coasts of Iran and Pakistan and results of numerical modeling. *Ocean Engineering*, 35(8-9):774–786. 1
- Heidarzadeh, M. and Satake, K. (2014). Possible sources of the tsunami observed in the northwestern Indian Ocean following the 2013 September 24 Mw 7.7 Pakistan inland earthquake. *Geophysical Journal International*, 199(2):752–766. 4
- Hoechner, A., Babeyko, A. Y., and Zamora, N. (2016). Probabilistic tsunami hazard assessment for the Makran region with focus on maximum magnitude assumption. *Natural Hazards and Earth System Sciences*, 16(6):1339–1350. 1, 3
- Horspool, N., Pranantyo, I., Griffin, J., Latief, H., Natawidjaja, D. H., Kongko, W., Cipta, A., Bustaman, B., Anugrah, S. D., and Thio, H. K. (2014). A probabilistic tsunami hazard assessment for Indonesia. *Natural Hazards and Earth System Sciences*, 14(11):3105–3122. 3
- Ide, S., Baltay, A., and Beroza, G. C. (2011). Shallow dynamic overshoot and energetic deep rupture in the 2011 M w 9.0 Tohoku-Oki earthquake. *Science*, 332(6036):1426–1429. 2
- Lay, T., Ammon, C. J., Kanamori, H., Yamazaki, Y., Cheung, K. F., and Hutko, A. R. (2011). The 25 October 2010 Mentawai tsunami earthquake (Mw 7.8)

- and the tsunami hazard presented by shallow megathrust ruptures. *Geophysical Research Letters*, 38(6):L06302. 2
- Lin, I.-C. and Tung, C. C. (1982). A preliminary investigation of tsunami hazard. *Bulletin of the Seismological Society of America*, 72(6A):2323. 3
- Liu, P. L.-F., Woo, S.-B., and Cho, Y.-S. (1998). Computer Programs for Tsunami Propagation and Inundation. Technical report, School of Civil and Environmental Engineering, Cornell University. 4
- Musson, R. (2009). Subduction in the Western Makran: the historian’s contribution. *Journal of the Geological Society*, 166(3):387–391. 2
- Okada, Y. (1985). Surface deformation due to shear and tensile faults in a half-space. *Bulletin of the Seismological Society of America*, 75:1135–1154. 4
- Okal, E. A. and Synolakis, C. E. (2008). Far-field tsunami hazard from mega-thrust earthquakes in the Indian Ocean. *Geophysical Journal International*, 172(3):995–1015. 1
- Parsons, T. (2008). Monte Carlo method for determining earthquake recurrence parameters from short paleoseismic catalogs: Example calculations for California. *Journal of Geophysical Research: Solid Earth*, 113(3):B03302. 3
- Priest, G., Goldfinger, C., Wang, K., Witter, R., Zhang, Y., and Baptista, A. (2009). Special paper 41: Tsunami hazard assessment of the northern Oregon Coast: A multi-deterministic approach tested at Cannon Beach, Clatsop County, Oregon. *AGU Fall Meeting Abstracts*, pages 1–100. 3
- Rajendran, C. P., Rajendran, K., Shah-hosseini, M., Beni, A. N., Nautiyal, C. M., and Andrews, R. (2013). The hazard potential of the western segment of the Makran subduction zone, northern Arabian Sea. *Natural Hazards*, 65(1):219–239. 1, 2
- Rajendran, C. P., Ramanamurthy, M. V., Reddy, N. T., and Rajendran, K. (2008). Hazard implications of the late arrival of the 1945 Makran tsunami. *Current Science*, 95(12):1739–1743. 1
- Rashidi, A., Shomali, Z. H., Dutykh, D., and Keshavarz Farajkhah, N. (2018). Evaluation of tsunami wave energy generated by earthquakes in the Makran subduction zone. *Ocean Engineering*, submitted. 3
- Rehman, S. U., Khalid, M., Ali, A., and Abd El-Aal, A. E.-a. K. (2013). Deterministic and probabilistic seismic hazard analysis for Gwadar City, Pakistan. *Arabian Journal of Geosciences*, 6(9):3481–3492. 1
- Rikitake, T. and Aida, I. (1988). Tsunami Hazard Probability in Japan. *Bulletin of the Seismological Society of America*, 78(3):1268–1278. 3
- Ruiz, J. A., Fuentes, M., Riquelme, S., Campos, J., and Cisternas, A. (2015). Numerical simulation of tsunami runup in northern Chile based on non-uniform k_2 slip distributions. *Natural Hazards*, 79(2):1177–1198. 3, 6
- Satake, K. (2014). Advances in earthquake and tsunami sciences and disaster risk reduction since the 2004 Indian ocean tsunami. *Geoscience Letters*, 1(1):15. 2
- Smith, G., McNeill, L., Henstock, I. J., and Bull, J. (2012). The structure and fault activity of the Makran accretionary prism. *Journal of Geophysical Research: Solid Earth*, 117(B07407). 2
- Smith, G. L., McNeill, L. C., Wang, K., He, J., and Henstock, T. J. (2013). Thermal structure and megathrust seismogenic potential of the Makran subduction zone. *Geophysical Research Letters*, 40(8):1528–1533. 1, 4, 5, 12

- Smith, W. H. and Sandwell, D. T. (1997). Global sea floor topography from satellite altimetry and ship depth soundings. *Science*, 277(5334):1956–1962. [4](#)
- Somerville, P., Irikura, K., Graves, R., Sawada, S., Wald, D., Abrahamson, N., Iwasaki, Y., Kagawa, T., Smith, N., and Kowada, A. (1999). Characterizing Crustal Earthquake Slip Models for the Prediction of Strong Ground Motion. *Seismological Research Letters*, 70(1):59–80. [4](#)
- Sørensen, M. B., Spada, M., Babeyko, A., Wiemer, S., and Grünthal, G. (2012). Probabilistic tsunami hazard in the Mediterranean Sea. *Journal of Geophysical Research: Solid Earth*, 117(B1):B01305. [3](#)
- Suppasri, A., Shuto, N., Imamura, F., Koshimura, S., Mas, E., and Yalciner, A. C. (2013). Lessons Learned from the 2011 Great East Japan Tsunami: Performance of Tsunami Countermeasures, Coastal Buildings, and Tsunami Evacuation in Japan. *Pure and Applied Geophysics*, 170(6-8):993–1018. [2](#)
- Tang, L., Chamberlin, C., Tolkova, E., Spillane, M., Titov, V. V., Bernard, E. N., and Mofjeld, H. O. (2006). Assessment of Potential Tsunami Impact for Pearl Harbor, Hawaii. *NOAA Technical Memorandum OAR PMEL-136*, 2984(August):1–42. [3](#)
- Wang, X. and Liu, P. L. F. (2005). A numerical investigation of Boumerdes-Zemmouri (Algeria) earthquake and Tsunami. *CMES - Computer Modeling in Engineering and Sciences*, 10(2):171–183. [4](#)
- Wang, X. and Liu, P. L.-F. (2006). An analysis of 2004 Sumatra earthquake fault plane mechanisms and Indian Ocean tsunami. *Journal of Hydraulic Research*, 44(2):147–154. [4](#)
- Weichert, D. H. (1980). Estimation of the earthquake recurrence parameters for unequal observation periods for different magnitudes. *Bulletin of the Seismological Society of America*, 70(4):1337–1346. [5](#)
- Yamazaki, Y. and Cheung, K. F. (2011). Shelf resonance and impact of near-field tsunami generated by the 2010 Chile earthquake. *Geophysical Research Letters*, 38(12):L12605. [2](#)
- Yamazaki, Y., Lay, T., Cheung, K. F., Yue, H., and Kanamori, H. (2011). Modeling near-field tsunami observations to improve finite-fault slip models for the 11 March 2011 Tohoku earthquake. *Geophysical Research Letters*, 38(20):L00G15. [2](#)

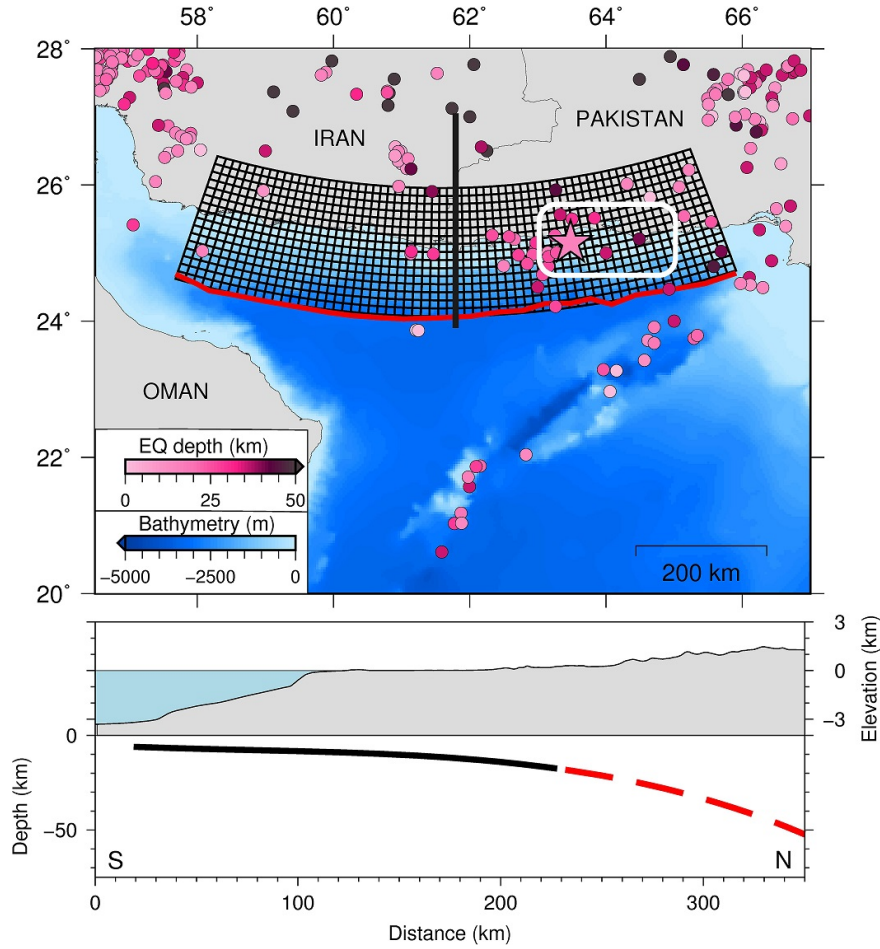


Fig. 1. Upper panel: Seismicity of the MAKRAN subduction zone (for $M_{4.0+}$ and between 1926 to 2016 from the ISC catalog). The star shows the epicenter of 1945 M_w 8.1 MAKRAN earthquake. The white outline represents the estimate of the approximate rupture area of the 1945 event (Byrne et al., 1992). The color of circles indicates the depth of events. The red line is the deformation front by Smith et al. (2013). The thick black line orthogonal to the deformation front denotes the cross-section. The non-planar mesh is the rupture geometry. Lower panel: Cross-section of the fault geometry (black line) and the palte interface (dashed red line) from Smith et al. (2013).

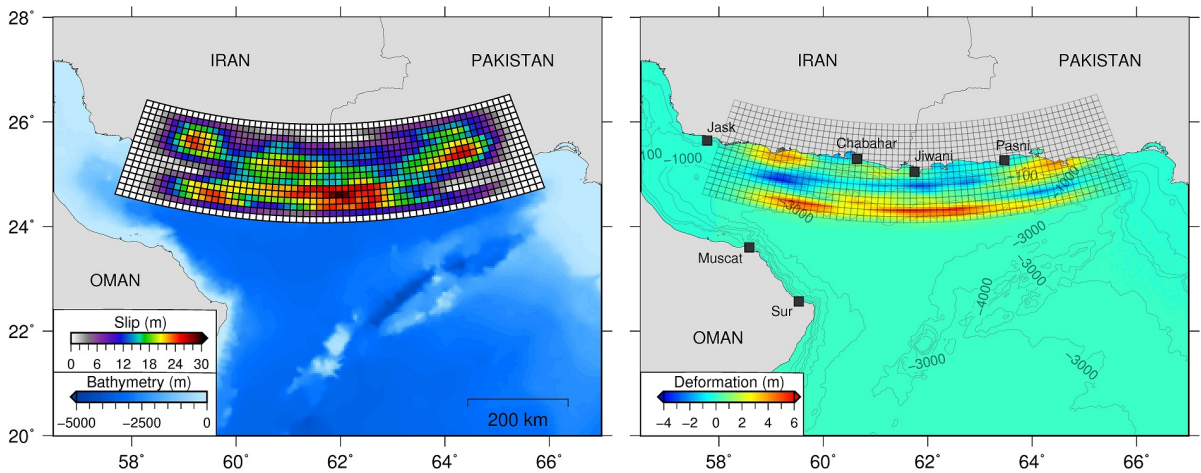


Fig. 2. An example of a k^{-2} slip model for the MAKRAN subduction zone (left panel) and the resulting vertical seafloor deformation (right panel). The non-planar mesh is the rupture geometry.

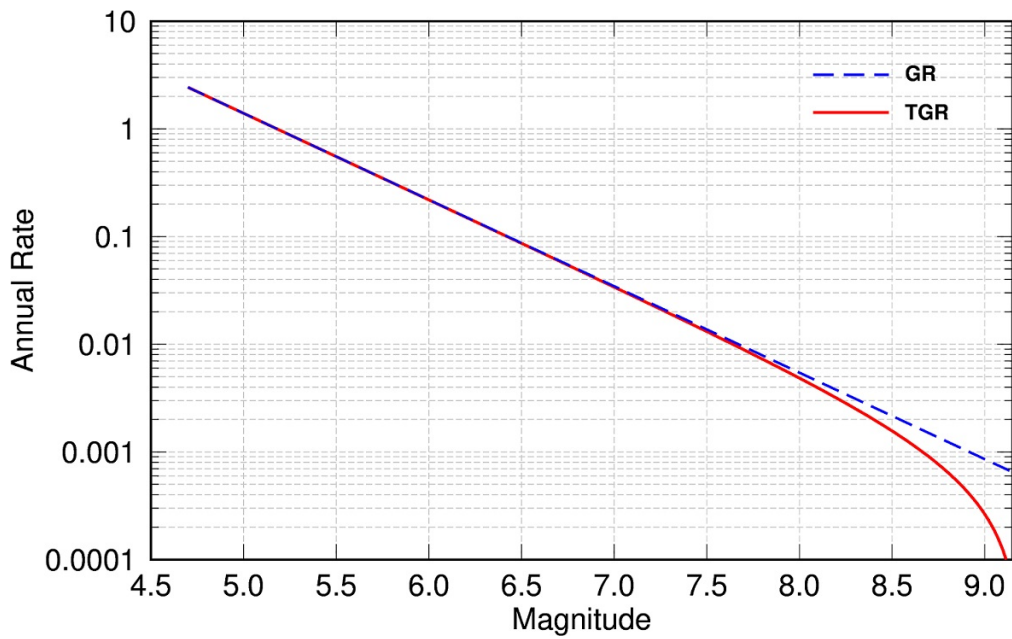


Fig. 3. Truncated GUTENBERG-RICHTER (TGR, solid red line) and GUTENBERG-RICHTER (GR, dashed blue line) relationships for the seismicity of MAKRAN subduction zone between 1926-2016 from the ISC Catalog.

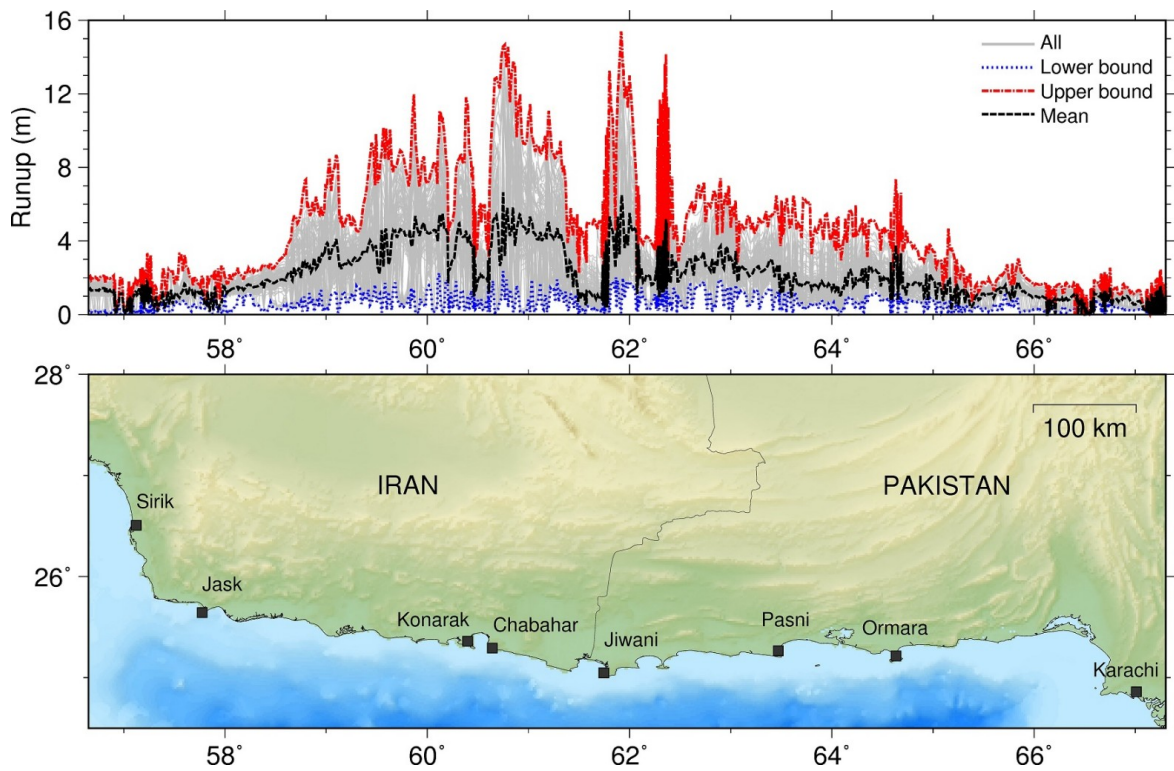


Fig. 4. Run-up distributions simulated in this study (gray lines) and mean (black dashed line), lower (blue dotted line) and upper (red dot-dashed line) run-up bounds along the coastlines of IRAN and PAKISTAN.

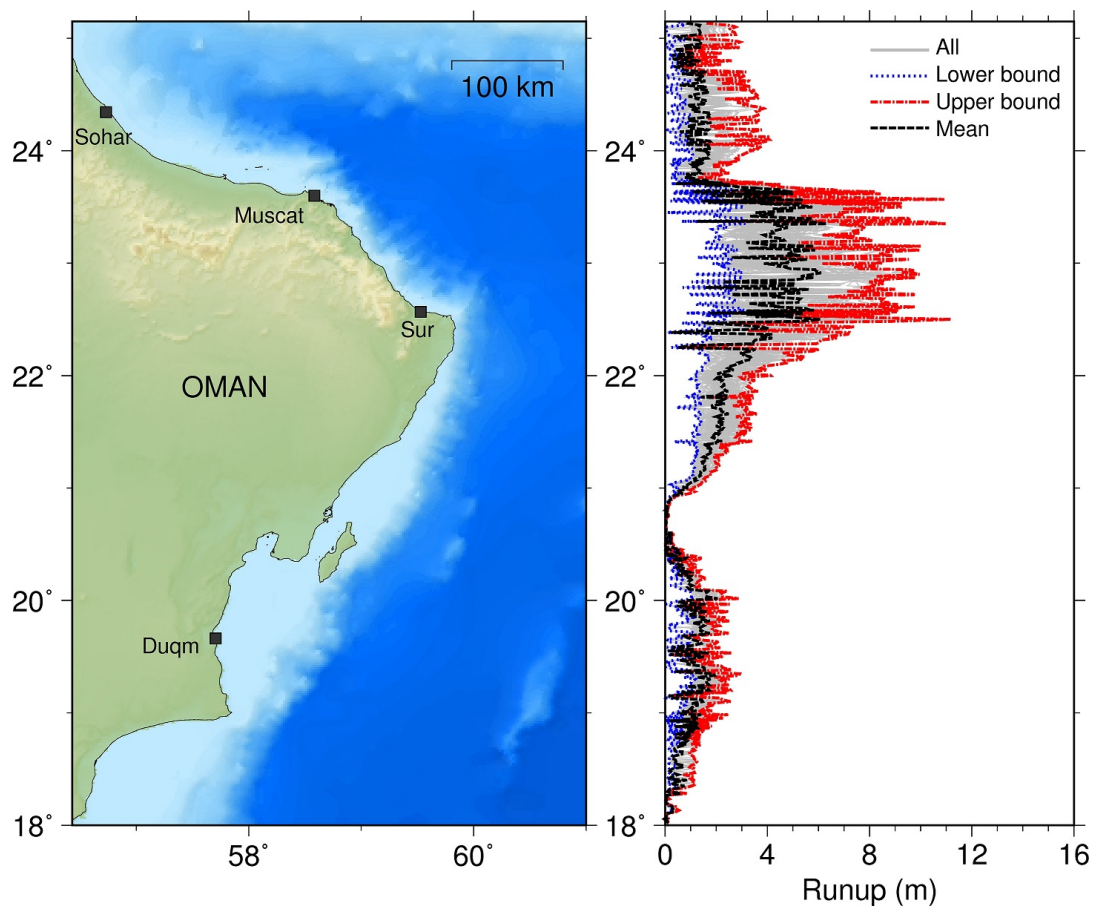


Fig. 5. Run-up distributions simulated in this study (gray lines) and mean (black dashed line), lower (blue dotted line) and upper (red dot-dashed line) run-up bounds along the coastline of OMAN.

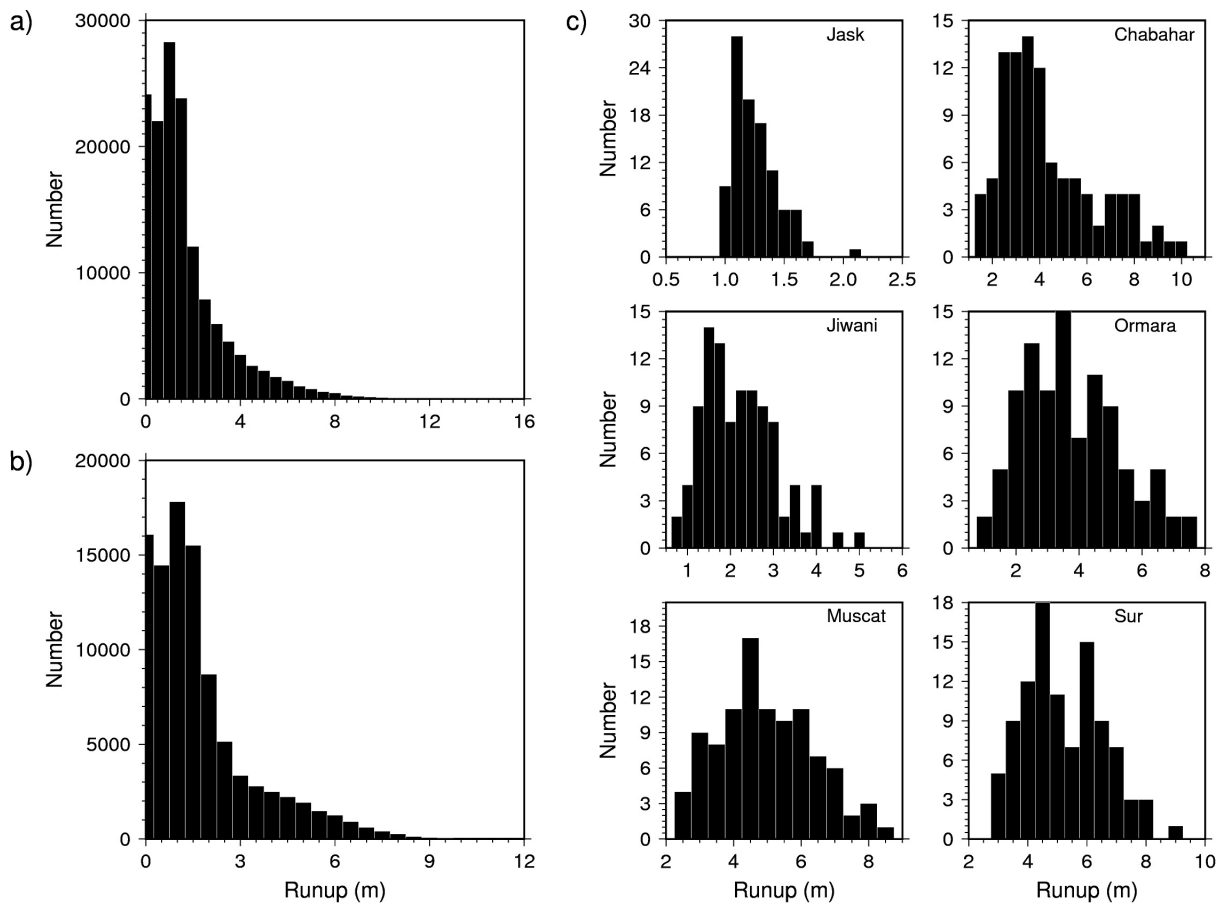


Fig. 6. Histograms of run-up heights along the coastlines of IRAN – PAKISTAN (a) and OMAN (b) and for selected ports (c).

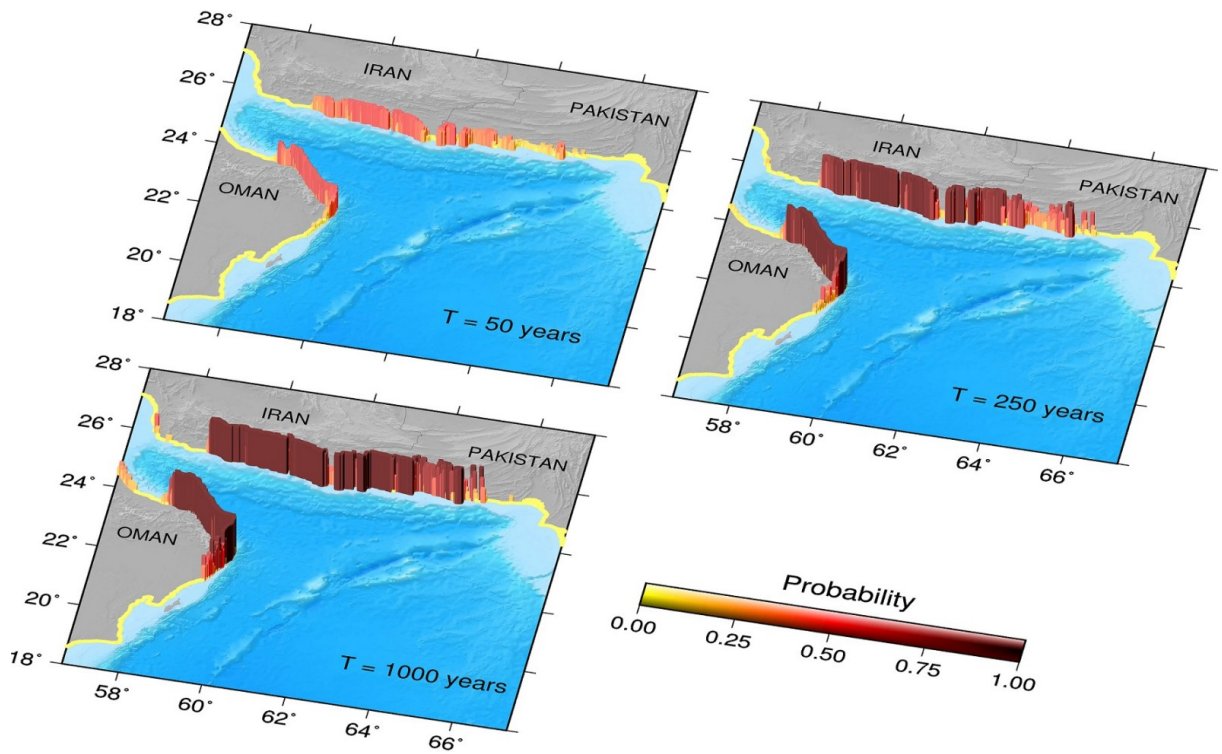


Fig. 7. Probability of exceeding 3 m in time periods of 50, 250 and 1000 years along the coasts of IRAN, PAKISTAN and OMAN.

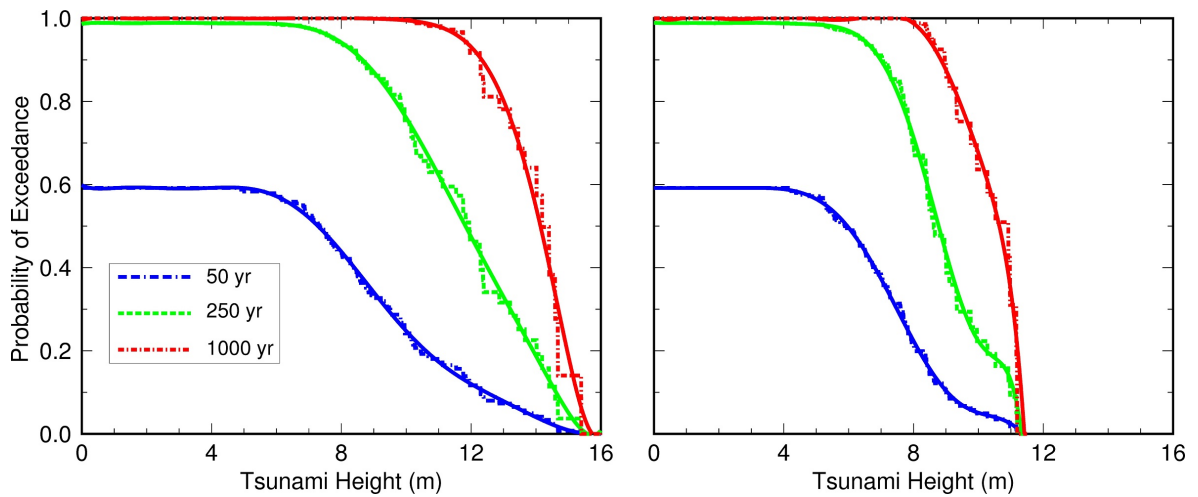


Fig. 8. Probability of exceeding different wave heights at one or more locations along the coastlines of IRAN – PAKISTAN (left panel) and OMAN (right panel). Solid lines indicate robust fitting.

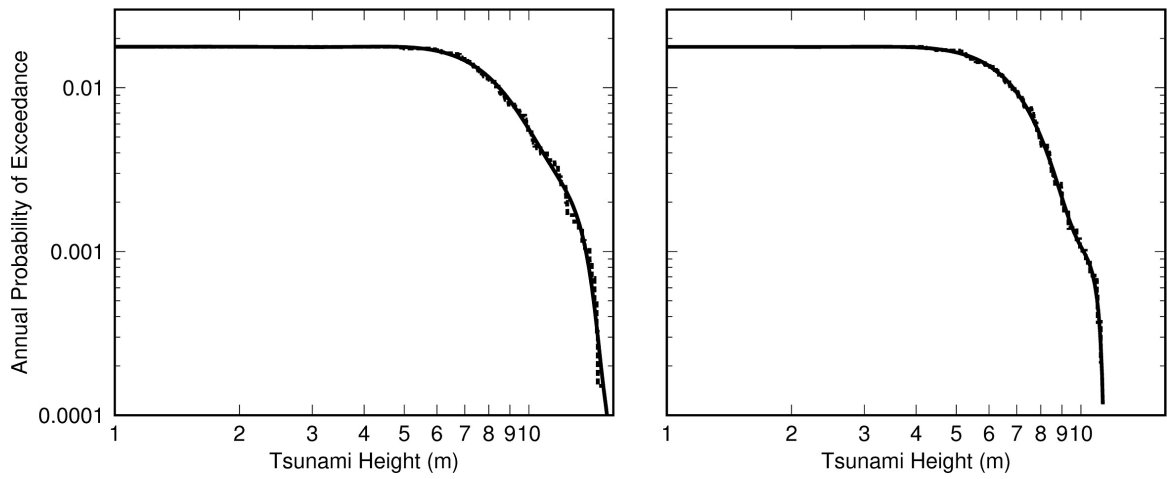


Fig. 9. Annual probability of exceeding different wave heights at one or more locations along the coastlines of IRAN – PAKISTAN (left panel) and OMAN (right panel). Solid lines indicate robust fitting.